Glass Elasticity from Particle Trajectories

Christian L. Klix, Florian Ebert, Fabian Weysser, Matthias Fuchs, Georg Maret, and Peter Keim

University of Konstanz, D-78457 Konstanz, Germany

Using positional data from video microscopy of a two-dimensional colloidal system and from simulations of hard disks, we determine the wave-vector-dependent elastic dispersion relations in glass. The emergence of rigidity based on the existence of a well defined displacement field in amorphous solids is demonstrated. Continuum elastic theory is recovered in the limit of long wavelengths which provides the glass elastic shear and bulk modulus as a function of temperature. The onset of a finite static shear modulus upon cooling marks the fluid-glass transition in an intuitive and unique way.

While fluids flow with a finite viscosity, solids respond elastically to deformation. At the glass transition, a super-cooled liquid transforms into a disordered solid which possesses mechanical rigidity to shear deformations. The corresponding elastic constant is the shear modulus μ [1]. In crystalline solids, shear rigidity results from the long-ranged correlations of displacements heralding the breaking of translational invariance. The transverse acoustical displacements are the Goldstone modes, whose (squared) amplitude scales with thermal energy in the equipartition theorem.

Yet, the emergence of rigidity at the glass transition, when an amorphous solid forms, remains poorly understood. Obviously, the disorder makes it a subtle fundamental problem to apply the concepts of spontaneous breaking of translational symmetry and of Goldstone modes. Already on the macroscopic level, different predictions exist for the behavior of the shear modulus μ when an amorphous solid forms. It has been predicted to jump discontinuously by mode coupling theory [2,3] or to increase continuously from zero by replica theory [4,5]. Such a continuous power-law increase from zero holds at the formation of a random gel, where a microscopic theory has established the link between the modulus and the Goldstone modes [6]. Also in the theory of granular systems, critical fluctuations close to point J (which is the density where a random athermal system becomes jammed) cause a characteristic algebraic increase of the shear modulus μ from zero [7]. A more recent calculation in replica theory again finds a jump in shear modulus at the glass transition and identifies the displacement field of a disordered solid, necessary to discuss elastic acoustic modes. [8]. Definitions of displacement fields in disordered solids have already been given in Ref. [9], yet the equipartition theorem could not be established in this approach.

Colloidal dispersions offer the unique possibility that the particle trajectories can be observed by video microscopy and thus are ideally suited to study displacements microscopically. In recent work on colloidal glass [10–12], the covariance matrix of the particle displacements was

obtained, and the mechanical density of states and the associated local modes were studied. But the shear modulus and the elastic dispersion relations were not obtained. Up to now, only in crystalline colloidal solids, the equipartition theorem provided a route to obtain them by microscopy [13,14].

In this Letter, we analyze the elastic properties for both an experimental 2D colloidal glass former and for simulation data of binary hard disks. We employ microscopy of displacement fluctuations, establish the equipartition theorem, and obtain the dispersion relations and elastic moduli. Our analysis is based on a quasiequilibrium description of the nonergodic glass state, which we derive under the assumption of a kinetic glass transition. The moduli are derived from thermally excited modes in the small wave vector limit. A sudden rise in the shear modulus marks the onset of vitrification. This proves that rigidity emerges differently in glasses than in polymeric gels and jammed granulates.

Here we briefly summarize our theoretical approach, which will be given in detail elsewhere. The relation $\dot{\mathbf{u}}_{\mathbf{q}}(t) = \mathbf{v}_{\mathbf{q}}(t)$ is the defining relation which introduces the collective displacement field $\mathbf{u}_{\mathbf{q}}(t)$; $\mathbf{v}_{\mathbf{q}}(t)$ is the familiar velocity field [15]. Fourier modes depending on wave vector $\mathbf{q}$ are considered to use translational invariance. Let time averaging be denoted by an overbar so that $\bar{r}_i$ is the average position of particle $i \in [1, N]$ during the time interval Δt, and the particle's displacement is $\mathbf{u}_i(t) = \mathbf{r}_i(t) - \bar{r}_i$. To order $\mathcal{O}[\mathbf{q} \cdot \mathbf{u}_i(t)]$, the field $\mathbf{u}_{\mathbf{q}}(t)$ follows by integration:

$$\mathbf{u}_{\mathbf{q}}(t) = \frac{1}{\sqrt{N}} \sum_{i=1}^{N} e^{i\mathbf{q} \cdot \bar{\mathbf{r}}_i} \mathbf{u}_i(t). \tag{1}$$

For this result to make sense, the particle displacements $\mathbf{u}_i(t)$ are required to remain bounded. For glass, this can be shown by using the Zwanzig-Mori equations of motion of the correlation functions [15], which are given in the Supplemental Material [16]. They are determined by stress kernels $\mathbf{G}(\mathbf{q}, t)$, which in the limit of vanishing q reduce to

the shear response $G(t)$ measured in macroscopic linear rheology [17]. We take glass to be a nonergodic state, so that the stress kernels, like density fluctuations [3,18], do not relax to equilibrium but take finite values at infinite time (index ∞), $\mathbf{G}(\mathbf{q}, t) \to \mathbf{G}_\infty(\mathbf{q})$, for $t \to \infty$. This is an idealization, as it requires that the structural relaxation time τ_α becomes infinite, while it (only) becomes larger than the measurement time in reality [19]. Then the equations of motion lead to displacement autocorrelation functions, whose equal time value obeys the equipartition theorem in glass [16]:

$$(\langle \mathbf{u}_\mathbf{q}^* \mathbf{u}_\mathbf{q} \rangle^{\text{glass}})^{-1} = \frac{q^2}{nk_BT}\left(\mathbf{G}_\infty(\mathbf{q}) + \frac{\hat{\mathbf{q}}\hat{\mathbf{q}}}{\kappa_q^T}\right) = \frac{1}{k_BT}\mathcal{D}(\mathbf{q}), \quad (2)$$

where $\kappa_q^T = S_q/(k_BTn)$ is the isothermal compressibility of the fluid with density n and structure factor S_q. The averaged squared displacements are given by elastic coefficients (the *dynamical matrix* $\mathcal{D}$), which are the frozen-in contributions in stress kernels. The superscript *glass* indicates that averaging is done in a restricted phase space set by the glassy state. As the so-obtained displacement fluctuations are ergodic, time and ensemble averages agree [20]; this was implicitly used in ansatz (1). The eigenvalues $\lambda_s(q)$ (the subscript s denotes polarization) of the dynamical matrix $\mathcal{D}$ are the *dispersion relations* and give the elastic spectrum of the amorphous system. In high symmetry crystals in 2D as well as in amorphous solids, the elasticity tensor possesses only two independent elements. These are the Lamé coefficients μ and λ of continuum elasticity theory. In two dimensions, μ gives the shear and $\mu + \lambda$ the bulk modulus, extracted from the transverse and longitudinal displacements $u_\perp(\mathbf{q})$ and $u_\parallel(\mathbf{q})$ in the long wavelength limit:

$$\frac{(2\mu + \lambda)}{nk_BT} = \lim_{\mathbf{q}\to 0}[q^2\langle|u_\parallel(\mathbf{q})|^2\rangle^{\text{glass}}]^{-1}, \quad (3)$$

$$\frac{\mu}{nk_BT} = \lim_{\mathbf{q}\to 0}[q^2\langle|u_\perp(\mathbf{q})|^2\rangle^{\text{glass}}]^{-1}. \quad (4)$$

In order to validate our prediction in Eq. (2) that the shear modulus $G_\infty = G(t \to \infty)$ derived from frozen-in stress correlations equals the one from static displacement fluctuations, $\mu = G_\infty$, we performed Brownian dynamics simulations of a binary mixture of hard disks in two dimensions [16,21]. Figure 1 shows the time-dependent shear stress correlation function $G(t)$ for (area) packing fractions ϕ close to the glass transition. The mode coupling glass transition was determined as $\phi_c \approx 0.796$ [21]. The $G(t)$ exhibit a two-step relaxation process with a finite amplitude of the final (so-called α) process. It decays only for times comparable to the structural relaxation time τ_α. Conventionally, it is obtained from fitting, e.g., a Kohlrausch law to the final decay [19,22]. When, upon raising ϕ, the time τ_α increases beyond the observation window, a finite *frozen-in* amplitude remains which is G_∞.
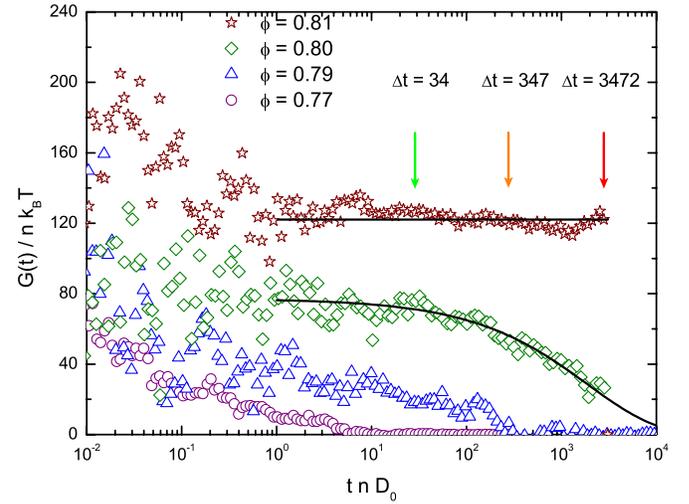

FIG. 1 (color online).   Shear modulus $G(t)$ from simulations of a glass forming mixture of hard disks for different packing fractions; D_0 is the dilute diffusion constant. Arrows indicate the length Δt of the trajectories, used to calculate the displacement fluctuations used in Fig. 2. At $\phi = 0.81$, a horizontal bar marks the plateau value $G_\infty = 124nk_BT$. At $\phi = 0.80$, a Kohlrausch law $G_\infty e^{-(t/\tau_\alpha)^\beta}$ is fitted to the final decay; $G_\infty = 77nk_BT$, $\tau_\alpha = 1900nD_0$, and $\beta = 0.60$.

Figure 1 shows that at intermediate times in the supercooled fluid, and in the glass, the shear elastic constant is finite.

Yet the simulations in Fig. 1 are very demanding so that earlier ones remained inconclusive on G_∞ [23], which advocates the more efficient method to correlate the displacement fluctuations. Quite intuitively, we use the time-averaged center of the trajectory as the *equilibrium* site of a particle. Its displacement is determined relative to this position as a function of time [24]. This goes beyond 3D crystals, where lattice sites can be used. The latter is unfeasible in amorphous solids as well as in 2D crystals where strict long-range translational order is spoiled due to Mermin-Wagner fluctuations [25]. Arrows in Fig. 1 indicate the lengths Δt of different trajectories used to calculate the shear modulus μ from the displacement fluctuations according to Eq. (4). The expression for $\bar{r}_i$ holds as long as Δt is smaller than the relaxation time τ_α. The results for μ are shown in Fig. 2 for different Δt and ϕ. The comparison for the states at $\phi = 0.80$ and 0.81 shows that μ calculated from displacement fluctuations agrees with G_∞ calculated from the stress autocorrelation function. This verifies our theory. The modulus μ takes finite values as long as the structural relaxation time τ_α exceeds Δt, as can be seen from Fig. 1. Approaching the mode coupling glass transition at ϕ_c from above, μ softens but stays finite in Fig. 2. Note that the time scale in Fig. 1 is logarithmic: Because of the equidistant sampling used to measure $\langle|\mathbf{u}_\perp(\mathbf{q})|^2\rangle$, the final part of the time signal dominates. This explains that in Fig. 2 for $\phi = 0.80$ the
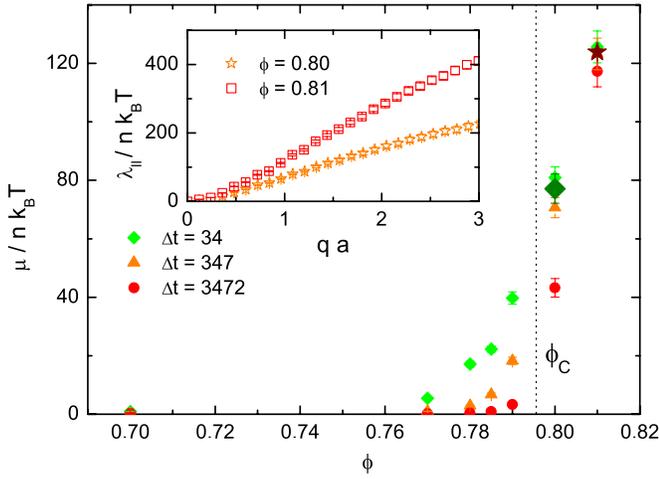
FIG. 2 (color online). Shear moduli μ (in nk_BT) from simulation as a function of area fraction ϕ. With increasing trajectory length (Δt given in units of nD_0), μ converges towards zero in the fluid. Crossing ϕ_c, μ jumps to a finite value for $\Delta t < \tau_\alpha$. $G_\infty = 124$ at $\phi = 0.81$ and $G_\infty = 77$ at $\phi = 0.80$ (dark star and green rhombus from Fig. 1) agree within errors with μ from Eq. (4). The inset shows the transverse glass dispersion relations.

measurement using $\Delta t = 3472$ is below the shorter ones. The final α process already affects this measurement. While this decay lacks a theoretical description, for the present context it suffices that it does not affect G_∞ [26]. On the fluid side, the modulus drops to very small values for Δt longer than the time scale of short time correlations. Because Eq. (4) measures a squared quantity, it can give only a positive value, which, however, converges to zero with increasing Δt in the fluid.

After having validated our method, we apply it to the experimental 2D colloidal glass. The system consists of a binary mixture of superparamagnetic polystyrene spheres confined to a flat water-air interface [27]. The species A (diameter $\sigma = 4.5$ μm) and B ($\sigma = 2.8$ μm) have a relative concentration of $\xi = N_B/(N_A + N_B) \approx 45\%$, where N_A and N_B are the number of particles of both species in the field of view. An external magnetic field H, perpendicular to the interface, lets us control the particle interactions *in situ*. This is expressed by the dimensionless coupling parameter

$$\Gamma = \frac{\mu_0}{4\pi} \frac{H^2(\pi n)^{3/2}}{k_BT} [\xi\chi_B + (1-\xi)\chi_A]^2, \qquad (5)$$

which acts as an inverse temperature. n denotes the 2D number density computed via Voronoi tessellation. $\chi_{A,B}$ is the susceptibility of species A and B. Video microscopy and digital image analysis provide the position of individual particles as a function of time.

In Fig. 3, the measured dispersion relations are shown for different interaction parameters Γ. Filled and empty symbols represent spring constants for longitudinal and transverse modes, respectively. The existence of transverse
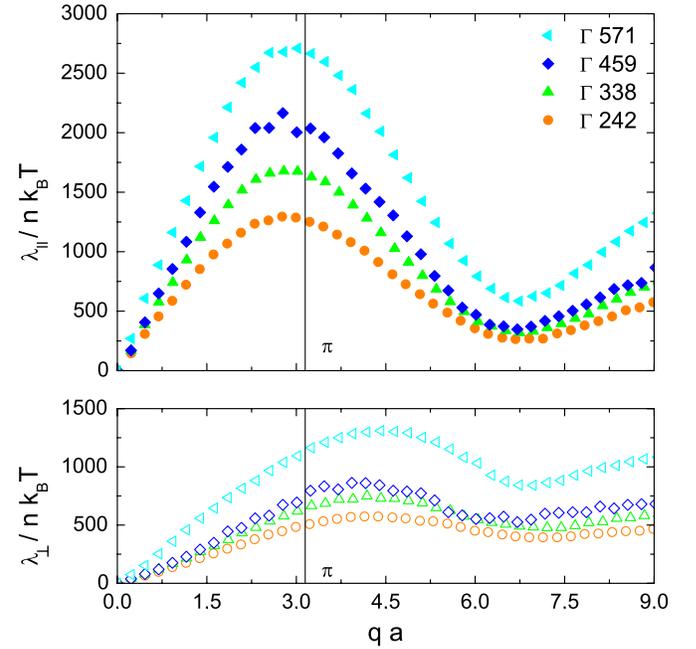

FIG. 3 (color online). The longitudinal (up) and transversal (bottom) dispersion relation of 2D colloidal glass for different interaction parameters Γ (inverse temperatures) as extracted from the displacements of particles from their time-averaged positions. Filled and empty symbols represent longitudinal and transverse polarizations, respectively.

elastic modes signals the solid. The small noise in the measured curves is remarkable and unexpected based on the complicated eigenvalue and eigenvector structure of the covariance matrices obtained from the instantaneous displacements in real space [10–12]. The Fourier-transformed displacements introduced in (1) apparently are a good set of modes. Their dispersion correlates with the mean particle separation a defined from the density $a^2n = 1$ revealing to the short-range order of the glass. The growing amplitude of the curves for increasing Γ reflects the expected stiffening of the system upon cooling.

From the dispersion relations, the moduli can be obtained via Eqs. (3) and (4). We chose an intermediate regime ($0.8 < qa < 2.0$) for the extrapolation $q \to 0$ where the data for linear regression fit best [13,28]. As the time interval Δt enables us to differentiate between high frequency and low frequency moduli, we discuss the dependence on Δt first. Reducing Δt (corresponding to high frequencies), Fig. 4 clearly indicates the expected growth of the shear modulus for both typical fluid ($\Gamma = 169$) and solid ($\Gamma = 394$) states. These results are consistent with Ref. [29]. At the same time, we see that for long sampling times Δt, its exact value makes no significant difference for computing the shear modulus. This is marked by a plateau (blue dashed line in Fig. 4). The plateau is more stable than the one in the mean squared displacement [30,31], which is already affected by the α process at a correlation time τ_α^{MSD} of about a few 10^5 s (inset in Fig. 4). The
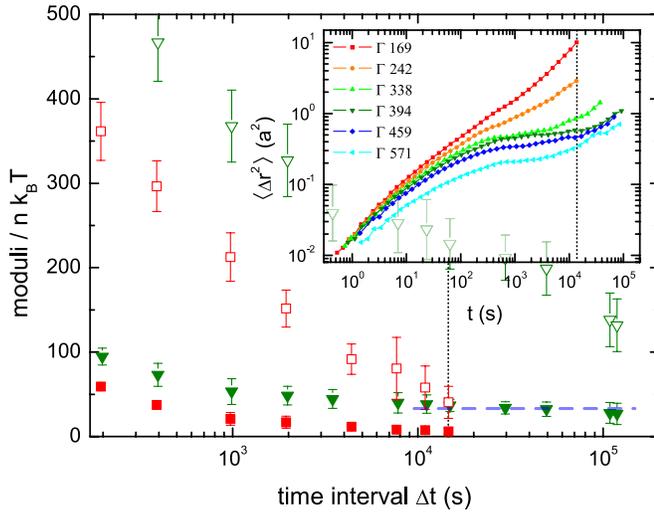
FIG. 4 (color online). The shear μ (filled symbols) and bulk modulus $\lambda + \mu$ (empty symbols) depending on sampling time Δt are shown for a glassy ($\Gamma = 394$, triangles) and a fluid state ($\Gamma = 169$, squares). For short trajectories Δt, the moduli increase. On long time scales, μ (green filled triangles) does not change in the glass (blue dashed line gives the best fit), whereas it has decayed for the fluid (red filled squares). In the glass, $\lambda + \mu$ decreases at long times when $\Delta t \approx \tau_\alpha$. The inset shows the mean squared displacement for different temperatures. The dashed vertical line indicates the sampling time $\Delta t = 14\,400$ s.

plateau in the shear modulus, however, ranges from 10^4 up to 10^5 s (which is the longest experimental sampling time we measured). In Figs. 4 and 5, the bulk modulus is included. It stays finite in the fluid phase for large Δt as expected. But since the amplitude square of the longitudinal mode is 10 times smaller compared to the transverse one, it is more strongly affected by structural relaxations at τ_α (e.g., aging) and/or Mermin-Wagner fluctuations [25] known from 2D crystals and also by a finite particle resolution [28] (see the error bars of Fig. 5). Therefore we focus on the shear modulus in the following.

Figure 5 displays the measured temperature dependence of the moduli [32]. As expected, the shear modulus μ is zero in the fluid phase (first three data points). As we further cool down our sample, we find an onset of μ, indicating the beginning of vitrification where the system becomes rigid (indicated by the shading). The magnitude of μ compares well to a mode coupling calculation $\mu = 13nk_BT$ (dashed arrow in Fig. 5) [33]. With the given temperature resolution of the experimental data, we cannot decide unambiguously if the shear modulus jumps discontinuously (as we did with the simulation data). But Fig. 5 clearly marks the region of vitrification which was unknown for 2D amorphous systems with long-range particle interaction.

In conclusion, we have shown that video microscopy allows us to obtain the elastic dispersion relation of an amorphous solid directly from the spatially Fourier transformed displacement fields. The classical equipartition
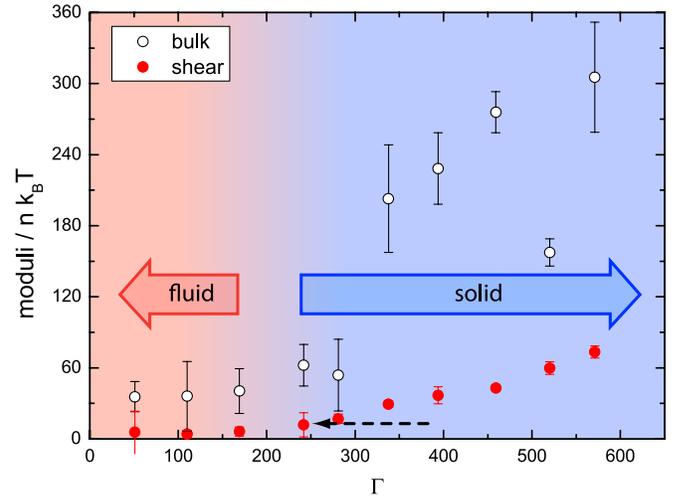

FIG. 5 (color online). At $\Gamma \approx 200$, we find an onset of the shear modulus (red filled circles) marking the temperature where the system starts to undergo vitrification. By cooling the system below T_g (increasing Γ), growing spring constants lead to an increase in stiffness. The arrow indicates the value of a mode coupling calculation at its transition temperature.

theorem holds, and in the long wavelength limit we can extract the elasticity from the dispersion relation. A finite quasiequilibrium shear modulus marks the onset of vitrification in the experimental 2D system. With simulation data we were able to show that this transition is discontinuous (unlike in granular systems or gels). Our work establishes microscopy of displacements as a novel spectroscopic technique in supercooled liquids and glasses. This is of especial interest in soft matter systems where the classical definition using a viscosity $\eta > 10^{12}$ Ns/m^2 does not hold.

[1] L. D. Landau, L. P. Pitaevskii, E. M. Lifshitz, and A. M. Kosevich, *Theory of Elasticity* (Butterworth-Heinemann, London, 1986), 3rd ed., pp. 142–144.
[2] E. Leutheusser, Phys. Rev. A **29**, 2765 (1984).
[3] W. Götze, Z. Phys. B **60**, 195 (1985).
[4] H. Yoshino and M. Mezard, Phys. Rev. Lett. **105**, 015504 (2010).
[5] H. Yoshino, J. Chem. Phys. **136**, 214108 (2012).
[6] S. Mukhopadhyay, P. M. Goldbart, and A. Zippelius, Europhys. Lett. **67**, 49 (2004).
[7] C. S. O'Hern, L. E. Silbert, A. J. Liu, and S. R. Nagel, Phys. Rev. E **68**, 011306 (2003).
[8] G. Szamel and E. Flenner, Phys. Rev. Lett. **107**, 105505 (2011).
[9] I. Goldhirsch and C. Goldenberg, Eur. Phys. J. E **9**, 245 (2002).
[10] A. Ghosh, V. K. Chikkadi, P. Schall, J. Kurchan, and D. Bonn, Phys. Rev. Lett. **104**, 248305 (2010).
[11] D. Kaya, N. L. Green, C. E. Maloney, and M. F. Islam, Science **329**, 656 (2010).

[12] K. Chen, W. G. Ellenbroek, Z. Zhang, D. T. N. Chen, P. J. Yunker, S. Henkes, C. Brito, O. Dauchot, W. van Saarloos, A. J. Liu, and A. G. Yodh, Phys. Rev. Lett. **105**, 025501 (2010).

[13] H. H. von Grünberg, P. Keim, K. Zahn, and G. Maret, Phys. Rev. Lett. **93**, 255703 (2004).

[14] D. Reinke, H. Stark, H. H. von Grünberg, A. B. Schofield, G. Maret, and U. Gasser, Phys. Rev. Lett. **98**, 038301 (2007).

[15] J. P. Hansen and I. R. Mcdonald, *Theory of Simple Liquids* (Academic, London, 2006).

[16] See Supplemental Material at http://link.aps.org/supplemental/10.1103/PhysRevLett.109.178301 for technical details of the theoretical approach and of the simulations.

[17] M. Siebenbürger, M. Fuchs, and M. Ballauff, Soft Matter **8**, 4014 (2012).

[18] W. Götze and M. R. Mayr, Phys. Rev. E **61**, 587 (2000).

[19] C. A. Angell, J. Non-Cryst. Solids **102**, 205 (1988).

[20] R. Kubo, J. Phys. Soc. Jpn. **12**, 570 (1957).

[21] F. Weysser and D. Hajnal, Phys. Rev. E **83**, 041503 (2011).

[22] Its finite amplitude contrasts with the power-law decay expected at the glass transition when G_∞ vanishes [4].

[23] J. L. Barrat, J. N. Roux, J. P. Hansen, and M. L. Klein, Europhys. Lett. **7**, 707 (1988).

[24] P. Keim, G. Maret, U. Herz, and H. H. von Grünberg, Phys. Rev. Lett. **92**, 215504 (2004).

[25] N. D. Mermin, Phys. Rev. **176**, 250 (1968).

[26] S. V. Adichtchev, St. Benkhof, Th. Blochowicz, V. N. Novikov, E. Rössler, Ch. Tschirwitz, and J. Wiedersich, Phys. Rev. Lett. **88**, 055703 (2002).

[27] F. Ebert, P. Dillmann, G. Maret, and P. Keim, Rev. Sci. Instrum. **80**, 083 902 (2009).

[28] The error bars for the simulations in Fig. 2 measure a statistical error. Since we cannot prepare identical representations (with identical histories) for the experimental system, the error bars of Figs. 4 and 5 stem from the linear regression of the extrapolation $q \to 0$ and the systematic error due to finite resolution in particle position (about 100 nm).

[29] Y. H. Jeong, Phys. Rev. A **36**, 766 (1987).

[30] H. König, R. Hund, K. Zahn, and G. Maret, Eur. Phys. J. E **18**, 287 (2005).

[31] S. Mazoyer, F. Ebert, G. Maret, and P. Keim, Europhys. Lett. **88**, 66 004 (2009).

[32] Δt was chosen to be $\Delta t \approx 14\,400$ s for the experimental data. It assures that we measure the glassy elasticity not in the high frequency region but at times shorter than τ_α.

[33] R. Seyboldt, D. Hajnal, F. Weysser, and M. Fuchs, Soft Matter **8**, 4132 (2012).